Thesis for the degree

Master of Science

Submitted to the Scientific Council of the

Weizmann Institute of Science

Rehovot, Israel

עבודת גמר (תזה) לתואר

מוסמך למדעים

מוגשת למועצה המדעית של

מכון ויצמן למדע

רחובות, ישראל

By

Amir Tal

מאת

אמיר טל

Estimating the aerodynamic resistance to heat and water vapour for use with the hydrological model TRAIN in semi-arid forest environments

הערכת ההתנגדות האווירודינמית למעבר חום ואדי-מים לשם שימוש עם תוכנת ההדמיה ההידרולוגית *TRAIN* ביערות צחיחים למחצה

Advisor:

Prof. Dan Yakir

מנחה:

פרופ' דן יקיר

December 2009

טבת התש"ע

Acknowledgements

I wish to extend my gratitude to my instructor, Prof. Dan Yakir, with whose insight, inspiration and knowledge showed me the way.

I am indebted to Drs. Eyal Rotenberg and Naama Raz-Yaseef for their critical thinking, and kind support, and to Prof. Lucas Menzel of the Heidelberg University for the use of the TRAIN model and the warm hospitality during my stay at the Kassel University.

Various folks around the department for Environmental Science and Energy Research have been indispensable and I am happy to thank them for their help. Hagai, Avraham, Emanuela and Ruthi always provided excellent technical assistance and advice in a friendly manner. I thank all of my friends and colleagues at the department– it's been a very memorable time.

Last but not least, I thank my parents, Tova and Benjamin, and my brothers, Amichai, Eran and Ehud, for their part in making this possible.

Declaration

All group members associated with the Yatir Forest research site have been involved in the maintenance and operation of the flux tower, under the direction of Dr. Eyal Rotenberg. The database of flux and meteorological data is maintained by Dr. Ruth Benmair. The model TRAIN was provided by Prof Lucas Menzel of Heidelberg University (formerly at Kassel University). Timeseries of micrometeorological data for use with the TRAIN model where supplied by Mrs. Ingrid Hausinger-Avalon.

All other work presented in this thesis is my own.

AT

Abstract

The overall resistance to mass transfer between leaf and the atmosphere is a key component in the control of heat, water and trace gas exchange at the land-air interface. Long-term micrometeorological data from the semi-arid forest of Yatir in Israel were analysed to obtain an estimate of the forest 'skin' temperature representing a combination of canopy and soil temperatures in this open canopy forest. The total aerodynamic resistance to heat and water vapour transport was calculated using the aforementioned temperature measurements. Aerodynamic resistance was low relative to other Mediterranean forest environments, with an annual average of 19 sm^{-1} and yearly minimum of 10 sm^{-1}. Model simulations of forest Evapotranspiration (ET) varied by up to 25% as a result of using different estimates of aerodynamic resistance. Our improved determination of aerodynamic resistance will enhance the ability of hydrological models to capture seasonal dynamics in ET (as well as the transport of other constituents in the forest-atmosphere system), assess the impact of afforestation on the hydrological water budget, and assess forest response to climate change.

תקציר

ההתנגדות הכוללת למעבר מסה בין עלווה לבין האוויר שמעל לחופת הצומח הינה רכיב מפתח בבקרה על חילופין של חום ואדי מים בין פני-קרקע ואטמוספרה. מצבת ארוכת טווח של נתונים מיקרו-מטאורולוגיים מן היער הצחיח-למחצה יתיר במרכזה של ישראל נותחה לשם קבלת סדרות של נתוני טמפרטורה עבור אדמת היער וחופת היער, מהן חושבו נתוני טמפרטורת פני-שטח משוקללת. נתון זה שימש לחישובה של ההתנגדות האווירודינמית למעבר חום ואדי מים בין היער לבין שכבת האוויר שמעליו. ההתנגדות האווירודינמית שנמדדה ביער הייתה נמוכה ביחס ליערות ים-תיכוניים אחרים, עם ממוצע שנתי של כ-19 שנ׳ למ׳ ומינימום שנתי של כ-10שנ׳ למ׳. הדמיות של כלל האידוי-דיות (Evapotranspiration - ET) מהיער אשר בוצעו במודל תוך שימוש במספר הערכות נפרדות של התנגדות אווירודינמית הניבו הערכות שונות עד כדי 25%, תוצאה המעידה על רגישות ההדמיה של אידוי-דיות להערכות של התנגדות אווירודינמית.

יכולתנו להעריך ביתר דיוק את ההתנגדות האווירודינמית תעצים את יכולתם של מודלים הידרולוגיים לדמות שינויים עונתיים באידוי-דיות, להעריך את השפעת פעולת הייעור על המאזן ההידרולוגי ולהעריך תגובת יער לשינויי אקלים.

Table of contents

(1) Introduction

(1.1) Rationale

Forests have long been the subject of human interest. Today we understand that they play a vital role in many areas including taking part in driving the Earth's climate, conserving land and shaping the landscape.

In the following work it has been my intent to study the exchange of both *water vapour* and *heat* between forest and overlying atmosphere, as these processes may have an important role in the effects of forests on the local, regional and global environments (Dolman *et al.*, 2004).

In recent years, mounting levels of the greenhouse gas of carbon dioxide in the atmosphere due to increased human activity have been linked to global warming of the Earth's surface and the low atmosphere (IPCC, 2001) . Further studies have shown concurrent changes in both the physical and biological Earth system including reduced sea ice cover, increased fire hazards in parts of the world (Pinol *et al.*, 1998), and a globally coherent shift in the onset of spring events (Parmesan & Yohe, 2003). Means for the mitigation of global CO_2 levels have been proposed which include fighting deforestation (Pacala and Socolow 2004) and planting of new forests in dryland areas.

Semi-arid lands comprise ca. 18% of the land surface on Earth, and are home to millions of people (WRI, 2002). Planting forests in semi-arid locations may turn semi-arid zones such as certain parts of the Mediterranean basin into potentially large carbon sinks giving these lands a significant role in future initiatives for carbon sequestration. Research in Yatir Forest, a semi-arid pine forest at the edge of its species distribution, has already proved that significant carbon storage in the semi-arid region is possible (Grunzweig *et al.*, 2007; Grunzweig *et al.*, 2003).

The impact of afforestation on the semi-arid region is unclear especially in terms of exchange of heat and water with the atmosphere and recharge of

underlying groundwater reservoirs, which are major sources of freshwater in Israel and worldwide (NGWA, 2009). With a projection of drier and hotter climate due to global warming, forests now enjoying a more temperate climate may be transformed to semi-arid conditions. In this aspect, studies conducted in Yatir Forest may reveal the impact of future climate on these forested lands, which have large economical as well as social and ecological importance.

(1.2) Earth systems modelling

Earth Systems Science is a science that deals with the needs to understand complex interactions among the atmosphere, biosphere, hydrosphere and lithosphere. The processes dealt with in the Earth Systems Science are more complex than could be dealt with within the conventional disciplines (e.g. ecology and meteorology). Developments from Earth System Science in the last few decades include examples in the context of climate (Sellers *et al.*, 1992; Sellers *et al.*, 1996) and the bio-geochemical cycling of matter (Charlson *et al.*, 1987).

Earth Systems Science embraces a systems approach. Often the processes dealt with cannot be dealt with using 'stand-alone' analytical equations. Numerical modelling in the earth systems is necessary to envision the system as a whole; to test interdependencies of its components and variables and to precisely account for mass, energy and momentum fluxes.

Lately, owing to the growing concern of global change, forest ecosystems have received ever more attention with emphasis on modelling efforts (Tiktak & van Grinsven, 1995; Verhoef & Allen, 1998). The need to account for the forest-atmosphere interaction has been addressed both at the process level (Charney *et al.*, 1977; Charney, 1975; Jarvis, 1976; Thom, 1972, 1975) and by using models such as Simple Biosphere (SiB; Sellers et al, 1986) and BATS (Dickinson, 1984). These models account for both processes concerning the vegetation growth and decay (carbon sequestration) and to heat, water vapour and momentum transfer with the atmosphere.

(1.3) Estimating Evapotranspiration: The Penman Monteith equation

The combination equation, introduced by Penman in 1948 (later augmented by Monteith, 1965; also known as the Penman-Monteith formula) is amongst the

most widely used and powerful formulae for loss of vapour from the surface to the atmosphere, in a process known as evapotranspiration (i.e. direct evaporation and transpiration through leaves). It combines the principles of energy conservation for plant canopies with the principles of transfer of water vapour due to the vapour pressure gradient. It is written as:

$$\mathrm{ET} = \frac{s\left(R_\mathrm{n} - \mathrm{G}\right) + \dfrac{C_a D}{r_H}}{\lambda\left(s + \gamma \dfrac{r_W}{r_H}\right)} \qquad (1.1)$$

With: ET evapotranspiration, $kg \cdot m^{-2} \cdot s^{-1}$;

s slope of the saturation vapour pressure vs. temperature curve ($kPa \cdot K^{-1}$);

Rn, G radiation and ground heat energy fluxes $W \cdot m^{-2}$;

$C_a = \rho \cdot Cp$; volumetric heat capacity of air, $kJ \cdot m^{-3} \cdot K^{-1}$; ρ = density of dry air, 1.2 $kg \cdot m^{-3}$;

Cp = specific heat of air, 1013 $J \cdot kg^{-1} K^{-1}$

$D = e_a^* - e_a$; vapour pressure deficit (VPD), kPa; e^*_a = saturation vapour pressure at air temperature, kPa; e_a = vapour pressure at height of measurement, kPa

r_H resistance to heat transfer, $s \cdot m^{-1}$;

λ latent heat of vaporisation, $2.26 \cdot 10^6$ $J \cdot kg^{-1}$;

γ psychrometric constant, 0.066 $kPa \cdot K^{-1}$;

r_W resistance to transfer of water, $s \cdot m^{-1}$.

The total resistance to the flow between leaf and a point above canopy actually occurs through a complex and branching network of resistances. Over the years different forms of the Penman-Monteith Formula have been introduced (Howell & Evett, 2004). These forms invariably differ by their treatment of the resistances involved. A short review of the resistance terms is hereby introduced followed by a description of the different forms of the Penman-Monteith Formula used.

1.3.1. Aerodynamic resistance

Heat transfer in air columns above crop (or forest) canopies is largely due to eddy diffusion and is reasonably well described in the literature (see, e.g., Jones (1992); Monteith and Unsworth (1990); Campbell and Norman, 1998). Within the bulk air above a canopy, wind speed usually assumes a logarithmic

profile that extends throughout the first 100m' of the boundary layer, driven by the horizontal momentum gradient. Like momentum, transfer of heat (and similarly for water vapour) in this layer follows *gradient-diffusion* and is strongly influenced by the wind speed and stability of the air profile. Aerodynamic resistance for momentum above the canopy is given by:

$$r_{aM} = \frac{\left(\ln\left(\frac{z-d}{z_0} \right) + \psi_m \right)^2}{\kappa u} \qquad (1.2)$$

z measurement height, m;

z_0 roughness length (height at which extrapolated wind speed equals zero; apparent sink for momentum), m;

d displacement height (displacement of the momentum sink due to vegetation morphology), m;

ψm instability correction function for momentum transfer, dimensionless;

κ von Karman constant, 0.41; dimensionless;

u wind speed, $m \cdot s^{-1}$.

The resistance terms for heat and mass may be derived from the resistance term for momentum as discussed below.

1.3.2. Relationships among heat, mass and momentum transfer in the atmosphere

Reynolds, in 1874, proposed a general theory for the transport of heat and momentum in turbulent fluids, proposing that both processes have resistances of similar magnitude, in what is known as the 'Reynolds' analogy'. Reynolds' analogy was taken further when in 1917 Schmidt proposed the existence of similarity between the resistances for heat, momentum and mass. Large parts of Reynolds' theory have been since confirmed, but controversy still remains regarding the similarity of the magnitude of the resistances. The similarity between the resistance for heat transfer and the resistance for mass poses particular interest for the modelling of evapotranspiration, as it allows the use of measurements of heat transfer for the estimation of evapotranspiration, as will be seen later in this work.

Many published experimental results suggest that there is a significant difference between the resistance to momentum transfer and that for heat in the vicinity of vegetated canopies, and offer formulae to correct momentum resistance data to heat resistance (e.g. Businger, 1971; Goudriaan, 1977;

Verma, 1989). Both theoretical and experimental work, as reviewed by Brutsaert (1984), show that heat and mass transfer are identical if the molecular diffusivity of the mass is similar to that of heat, i.e. approx. $2.2 \cdot 10^{-6}$ $m^2 s^{-1}$.

To accommodate for the differences in the resistances of heat and momentum and to obtain expressions for r-a for heat, it has been proposed (e.g., Verma 1989) to define a roughness length for heat:

$$z_{oh} = z_0 \exp(-\kappa B^{-1}) \tag{1.3}$$

With: z0h roughness length for heat, m';
z0 roughness length for momentum, m';
B^{-1} non-dimensional measure of the difference between z_{0h} and z_0

Since z_0 is considered the height at which the wind speed assumes zero (when extrapolating the logarithmic wind profile), it stems that z_{0h} is the height at which the apparent temperature profile above the vegetation reaches Tc, the canopy surface temperature. For typically permeable surfaces (e.g. most vegetated surfaces) B^{-1} is rather constant over a wide range of meteorological conditions but varies between different types of surface (Brutsaert 1984); a value on the order of 2.5 is considered both for heat and for water vapour. A general equation can now be arrived at for resistance for either heat or water vapour:

$$r_a = \frac{\left(\ln\left(\frac{z-d}{z_0}\right) + \psi_m\right)\left(\ln\left(\frac{z-d}{z_{0h}}\right) + \psi_h\right)}{\kappa u} \tag{1.4}$$

With: r-a aerodynamic resistance for scalar admixtures, $s \cdot m^{-1}$;
z0h roughness length for heat (apparent height of the sink for heat), m;
ψh instability correction function for heat transfer, dimensionless.

1.3.3. Boundary layer resistance

The flow directly adjacent to the surface of the transpiring leaves (similarly: to the soil surface) is less turbulent, and a larger resistance term is necessary to describe heat and vapour transfer. This resistance is termed the boundary layer resistance (r-b). Dimensional analysis of r-b for heat yields an expression of the form (Monteith and Unsworth, 1990):

$$r_{bH} = \frac{d}{\kappa \cdot \mathrm{N_{ND}}} \tag{1.5}$$

With: d characteristic length, m

κ thermal diffusivity of air, m^2s^{-1}

N_{ND} a non-dimensional measure of the boundary layer depth. For heat it is the Nusselt number (Nu); for water vapour, CO_2, etc – the Sherwood number (Sh).

The size of Nu varies widely depending on the degree of turbulence and wind speed as well as on temperature gradients in the air adjacent to the surface.

The total resistance to heat between leaf and mixed layer above the canopy is represented in figure 1.1. Individual boundary layer resistances act in parallel to give an equivalent boundary layer resistance, which works in series with a bulk aerodynamic resistance. In equation form this is:

$$r_H = r_{aH} + r_{bH} \tag{1.6}$$

With: raH bulk air resistance ($s \cdot m^{-1}$)

r_bH parallel sum of the individual boundary resistances, r-b1, r-b2, etc, ($s \cdot m^{-1}$):

$$r_{bH} \cong \overline{r_b} \cdot LAI^{-1} \tag{1.7}$$

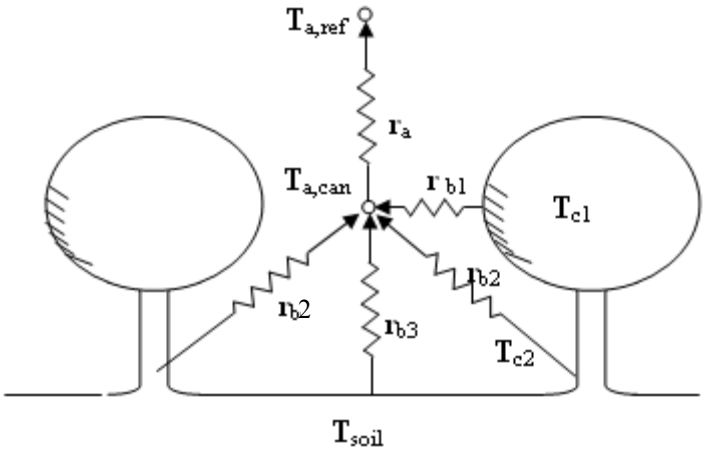

Figure 1-1: illustration of an idealised heat resistance network. Heat flow from surface elements (e.g. soil, bark, leaves) passes through boundary layers into the bulk air, from which it passes by eddy diffusion to the air above canopy. Soil and lower canopy elements are significant to the total release of heat.

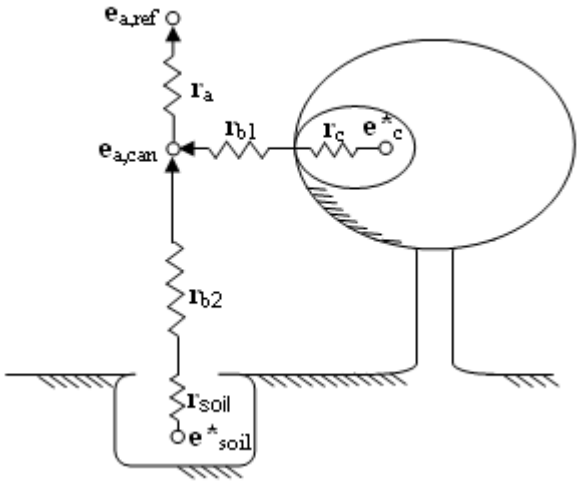

Figure 1-2: a resistance network to water vapour. Vapour passes from the pore space within the leaf (in the canopy) or the soil into the bulk air, from which it passes by eddy diffusion to the air above canopy. e= vapour pressure (kPa); e*=saturation vapour pressure (kPa).

1.3.4. Surface resistances

Evaporation from the liquid-gas interface within pores in the leaves (called stoma, singular: stomata) and the soil is controlled by forces which combine at the macroscopic scale to create the surface resistance to the flow. This is usually the largest component of the resistance to water vapour. Transpiration is a highly regulated form of evaporation occurring in plants. Plants may open and close stoma in response to environmental conditions such as humidity and light, but often this process is regulated by the rate of photosynthesis in leaves (Sellers *et al.*, 1992). As such, canopy resistance is a function of the exposure of green leaves in the canopy to light, net above-canopy solar radiation, water status at the root zone, as well as humidity of the air.

1.3.5. Modifications to the Penman Monteith formula

As in other works, equation 1.1 is modified in this work in order to account for the resistance terms r-h and r-w. The resistance to water vapour is assumed to be made up of two components – an aerodynamic resistance and a canopy (soil and/ or leaf) resistance acting in a row:

$$r_W = r_c + r_a \tag{1.8}$$

In addition, the resistance to heat is assumed equal to the aerodynamic component of the water vapour resistance, r-a:

$$r_H \approx r_{AW} \equiv r_a \tag{1.9}$$

Equation 1.1 then becomes:

$$\mathrm{ET} = \frac{s\left(R_\mathrm{n} - \mathrm{G}\right) + \dfrac{\rho_a c_p D}{r_a}}{\lambda\left[s + \gamma\left(1 + \dfrac{r_c}{r_a}\right)\right]} \tag{1.10}$$

This convention is used in the literature throughout, although boundary layer resistance to water vapour may be two fold that for heat (Sellers et al 1996). The modified Penman Monteith formula therefore conceptually divides r-b for water vapour in between the r-c and r-a parts. r-a used in the Penman-Monteith equation is therefore virtually equal to r_H.

1.3.6. Limitations to the Penman Monteith formula

The Penman Monteith equation inherently examines only 'one-way' interactions, such as the effects of humidity, temperature and radiation fields on the water vapour flux (ET). Increasing evidence shows that the opposite interactions (e.g. the effect of temperature and humidity fields on radiation) may not be neglected in all but the simplest cases.

The Penman-Monteith equation assumes a single flow-path for water emanating from the surface and likewise for heat, treating the surface as if it were 'one big leaf' (Howell & Evett, 2004); when dealing with natural vegetation, this is often a gross oversimplification as already shown in figures 1.1and 1.2.

Nevertheless, the Penman-Monteith equation has been extensively used including for some forest environments (e.g., Lindroth 1993) and may serve as a first approximation.

(1.4) Objectives

Evapotranspiration at the forest-atmosphere boundary is central to understanding the hydrology and ecology of forests in general and forests at the dry edge of their distribution in particular. The computer model TRAIN applies semi-empirical relationships for the estimation of both aerodynamic and canopy resistances which together comprise the resistance for water vapour transport. These relationships were calibrated against temperate grassland data and could not explain initial observations of the resistances in the Yatir Forest. Long-term micrometeorological data from the Yatir field site offered a unique opportunity to examine the dynamics of the actual resistances in the forest by the inverse method.

The goals of the research were therefore as follows:

1. To quantify and measure the aerodynamic resistance for water vapour in the open-canopy dry Yatir Forest, using the existing field research site in the forest and its extensive dataset;
2. To compare modelled aerodynamic resistance with observations, and analyse any discrepancies between them;
3. To offer an improvement of the representation and characterisation of aerodynamic resistance in semi-arid forest environments in TRAIN.

(2) Materials and methods

(2.1) Research site

Yatir Forest is a maturing 2800 ha afforestation site of mostly Allepo pine (*P. halepensis* Mill., אורן ירושלים in Hebrew) situated on sloping terrain some 25 km to the south of Hebron, 25 km north of Beersheba in central Israel (31°21′N, 35°03′E; height: 650 m above sea level). It is considered to be at the hot/dry edge of forests' distribution (Grunzweig *et al.*, 2007).

Being the largest afforestation site in the whole of Israel, it constitutes a large concentration of Allepo Pine, a Mediterranean pine species prone to growing in hot, dry climate (Maseyk *et al.*, 2008). The forest was planted on native shrubland consisting of mainly Thorny Burnet (*Sarcopoterium spinosum*) dwarf shrubs (Grunzweig *et al.*, 2007). Planting occurred mainly during 1964-1969, with several small additions continuing to this day. Tree density at the forest core is approx. 300 trees ha^{-1}, with mean tree height of 11 m, mean diameter at breast height (DBH) of 17 cm, and Leaf Area Index (LAI) of ~1.5 (Sprintsin *et al.*, 2007). The forest was thinned a few times in its life time (Grunzweig *et al.*, 2003).

From a climate perspective, Yatir Forest is a semi-arid forest ecosystem. Rainfall is low, averaging 290 mm annually (multiyear average) having fluctuated between 147 mm and 496 mm (Maseyk *et al.*, 2008). Rainfall occurs in sporadic showers during November - March, resulting in a long dry season (6–7 months). The average annual air temperature is 18.2°C, with mean daytime air temperatures ranging from 10°C in January to 25°C in July. Relative humidity, wind speed and solar radiation are given in figure 2-1.

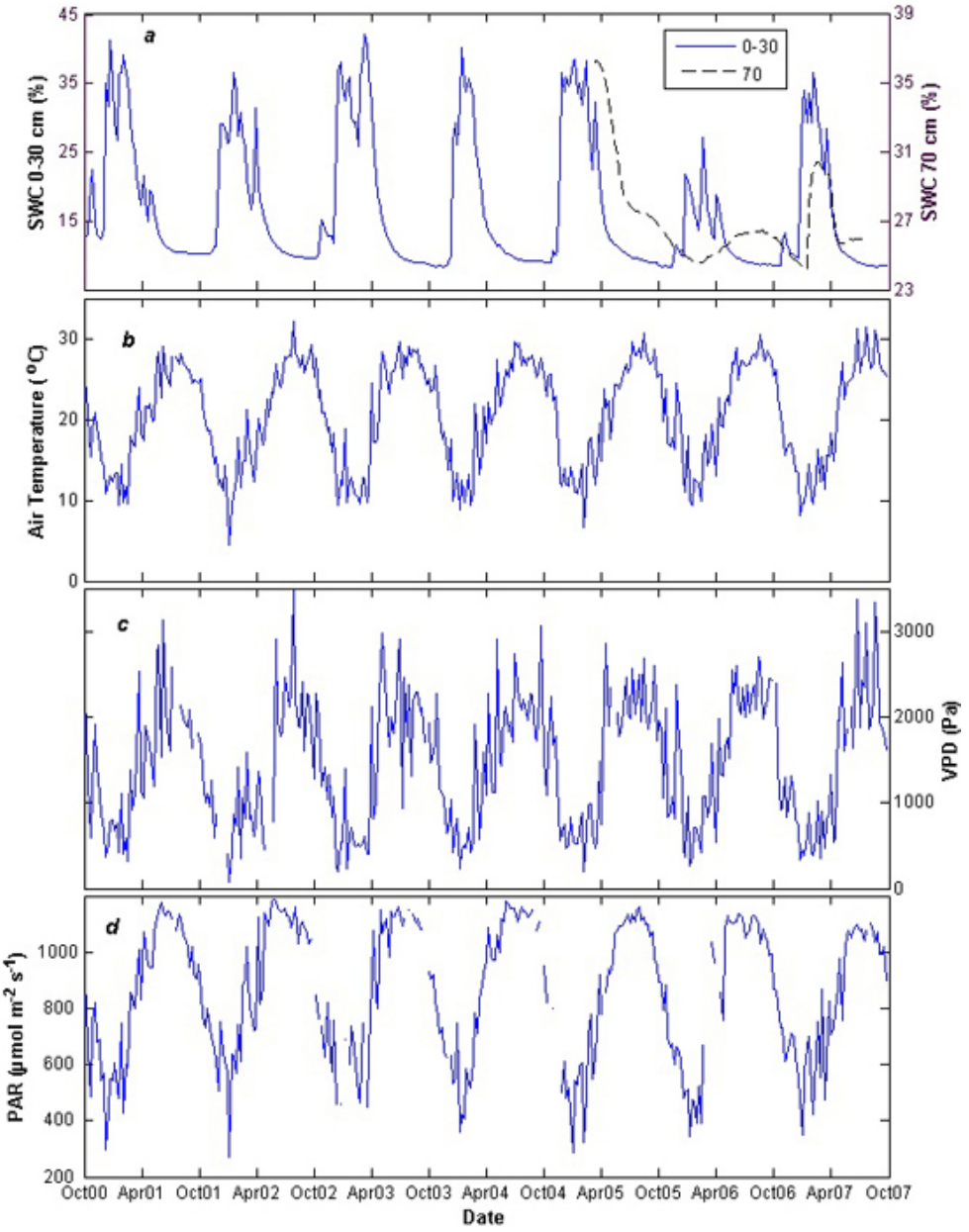

Figure 2-1: Weekly mean values of climatic parameters in Yatir: (a) Soil water content (SWC) at depths 0-30 cm and 70 cm; (b) Air Temperature; (c) Vapour pressure deficit (VPD); (d) Photosynthetic active radiation (PAR). Note that panel b to d report daytime values only.

Yatir Forest is among the sunniest forests on Earth, with incoming solar radiation averaging an annual 7.5 GJ m^{-2} (Rotenberg and Yakir, subm.). The aridity index (ratio of precipitation to potential evapotranspiration) is 0.2, which is at the lower limit for semi-arid climates. The soil is shallow and poor (0.2–1 m deep lithosol above chalk and limestone) with a deep (approx. 300 m) ground water table.

It was recently shown (Raz Yaseef, 2008) that water entering the system through precipitation is almost entirely lost through evapotranspiration; only a

small fraction is allowed to percolate. There is virtually no runoff from the forest (less than 5% of precipitation). Further, it was found that annually ca. 40% of evaporation originates from the understory and bare soil, leaving considerably little water for transpiration by the forest trees.

(2.2) Instrumentation at research site

All flux data for this study was collected from measurements performed at the R. Lewis and C. Wills Yatir Forest research site in the Yatir Forest. The site was established in April 2000 and provides flux measurement data since then. Flux measurement data is continuous and data transferred to a database at the Weizmann Institute of Science in Rehovot weekly. The main types of instrumentation relevant to this study are described:

a) **Eddy flux system**, consisting of a closed-path infrared gas analyser (LiCor Biosciences inc., Nebraska, USA) and a 3D sonic anemometer (Gill Instruments, UK), situated 9 m above canopy and 19 m above ground level (m.a.g.l). This system provides measurements of the vertical sensible heat flux (H), latent heat flux (LE), water vapour flux (ET) and CO_2 flux (Fc), as well as: air temperature at height of measurement (19 m.a.g.l), wind speed (u) and momentum flux (u_*^2).

b) **Radiation sensor array**, consisting of four hemispherical thermal infrared radiation sensors (4.0-100 μm; Eppley laboratory, Newport, USA), five shortwave (0.29 – 4 μm) radiation sensors (Kipp and Zonen, Delft, The Netherlands) and an auxiliary net radiation sensor (Kipp & Zonen, Delft, The Netherlands). The sensors are arranged in two identical sets each consisting of a down-facing PIR (infrared sensor) and CM21 (shortwave sensor), and an up-facing PIR and CM21. One such set of sensors is placed 4 m above canopy (14.5 m.a.g.l) while the other is placed below canopy level, at a height of 2 m.a.g.l. An auxiliary net radiation sensor, the NR-LITE, at 14.5 m.a.g.l, provides a back-up for net radiation measurements. An additional set of sensors measured photosynthetic active radiation (PAR radiation sensors; 0.4-0.7 μm) but was not used in this study.

c) **Meteorological instrumentation**: a T-type thermocouple array, measuring air temperature at heights of 1, 5, 9 and 13 m.a.g.l, on arms 2 m length extending from the flux tower; a rain gauge, situated 4m above canopy; wind sentries at 15 m, 6 m and 1 m; a relative humidity and air temperature sensor (Campbell Scientific), situated 4m above canopy.

d) **Soil heat flux system**: an array of sensors to continuously measure heat storage in the topsoil and the ground heat flux through the combined method (Agam *et al.*, submitted).

e) **Soil water sensor system**: an array of soil water sensors includes a spatially distributed set of TDR sensors (TRIME, Germany) which continuously measures soil water content (SWC) at depths of 5, 15, 30, 50 and 125 cm. In addition, a set of two sensors (Campbell Scientific) measures SWC averaged over the top 30 cm of ground (Raz Yaseef, 2008).

All sensors were connected via a multiplexer to data loggers (Campbell Scientific, Logan, USA).

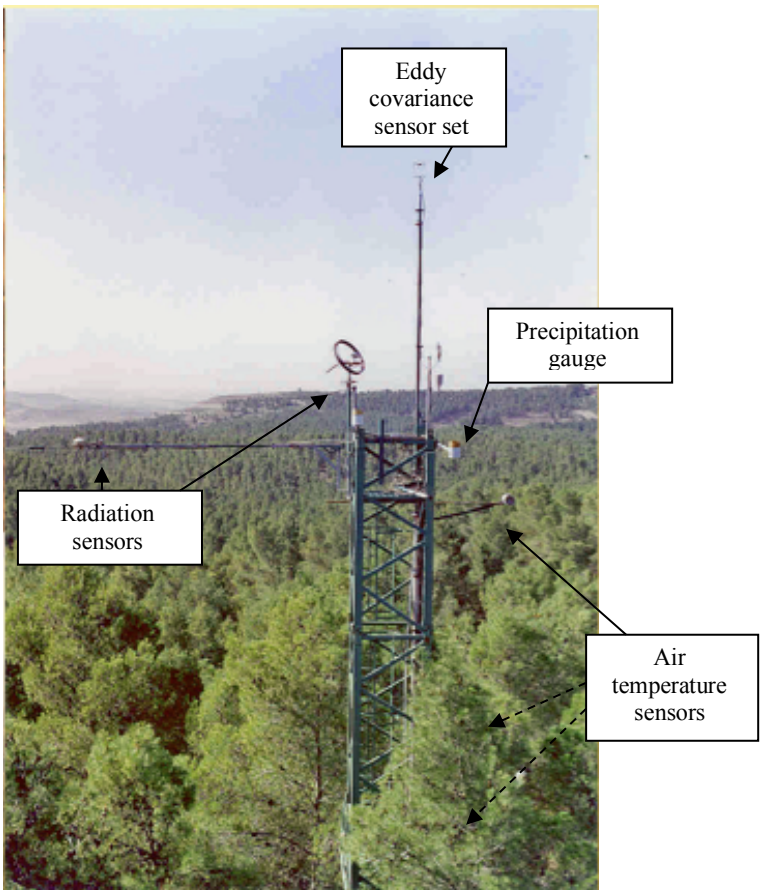

Figure 2-2: profile of the instrumental setup in the Yatir Forest research site, showing upper part of flux tower with instrumentation and upper radiation mast.

(2.3) Data collection, storage and processing

2.3.1. Data collection and storage

Flux data as well as meteorological data for the period of 1.1.2003 - 31.12.2004 were queried from the Yatir Forest site database at the Weizmann Institute. These data include: short- and longwave radiation; air and soil temperature at various heights; sonic anemometer temperature and wind speed measurements; top-of-canopy sensible and latent heat fluxes; soil heat flux; air pressure and humidity; precipitation and soil water content. Values reported here are based on ½ hour averages of values collected either by data loggers at 0.2 Hz, or by the EC system at 20 Hz.

2.3.2. Data processing

All data processing was performed on a personal computer (LG electronics, CPU: Intel Pentium M 1.4GHz~2.0GHz) using either Microsoft Excel (Microsoft corporation) for data averaging, filtering, summation, plotting,

graphing, data preparation and storage, or Matlab (the Mathworks group) used for the processes of gap filling, plotting and graphing of data.

All data queried were transformed into a file format compatible to Microsoft Excel and (if required) to Matlab compatible .mat files. Matlab scripts are given in appendix.

(2.4) The inverse method for obtaining r_a from eddy flux and temperature measurements

Based on the general formula for heat transfer by eddies in a fluid in motion:

$$H = \rho C_p \frac{T_a - T_{sur}}{r_{aH}} \tag{2.1}$$

An expression for the total resistance for heat transfer was obtained:

$$r_{aH} = \rho C_p \frac{T_a - T_{sur}}{H} \tag{2.2}$$

We term the estimate of r-a based on this equation, the *inverse method* for acquisition of aerodynamic resistance, as it uses the measured flux *(H)* to estimate r-a, which in turn is needed for modelling and estimating fluxes.

(2.5) Acquiring soil and canopy temperature from radiant energy measurements

Assessing the temperature of the forest surface elements (e.g. soil and leaf surfaces) is required for the application of the inverse method for the investigation of aerodynamic resistances.

Direct estimation of canopy surface-temperature is difficult to achieve, because of the spatial and temporal heterogeneities involved and the dynamic nature of plant canopies (Campbell & Norman, 1998). The radiometric temperature of a plant canopy (i.e. temperature estimated using a radiometric approach) may be obtained from the long-wave radiation emitted by the canopy (or, similarly, the soil) using the Stefan-Boltzmann equation:

$$L_c = \varepsilon_{L,c} \sigma T_c^4 + L_r \tag{2.3}$$

With:
- L_c long-wave irradiance ($W \cdot m^{-2}$);
- $\varepsilon_{L,c}$ mean long-wave emissivity of canopy (dimensionless);
- σ Stefan-Boltzmann constant ($W \cdot m^{-2} \cdot K^4$);
- L_r longwave radiation reflected off of the observed surfaces ($W \cdot m^{-2}$).

(2.6) The TRAIN ecosystem hydrology model

2.6.1. model description

We have adopted for parts of this study an operational hydrological model, TRAIN, developed by Menzel (1996). The model simulates the main hydrological processes occurring at the soil-vegetation-atmosphere interface. TRAIN may be run for plot-scale simulations (the local version) or for regional simulations (the regional version). Simulations may be executed deploying either hourly or daily time-steps for calculation. The basic hydrological unit in TRAIN is the plot, a homogeneous unit of land with an ascribed land-use type and vegetation cover. TRAIN was initially calibrated against empirical data from a temperate grassland (Menzel, 1996) and validated against data from sites in both Germany and Mongolia. The local version of TRAIN requires the following input meteorological data: radiation (either global, net or simply duration of sunshine), precipitation (total), wind speed, air temperature and the relative humidity, with the last three specified at a point above canopy level. Additional input data includes soil depth, soil-plant water relations (field capacity and permanent wilting point), initial soil moisture, and land cover classification (chosen from a pre-programmed set).

2.6.2. Model equations

Calculations are performed within specified 'modules' according to function: 1 – phenological processes; 2 – radiation balance; 3 – interception evaporation; 4 – soil evaporation; 5 – transpiration; 6 – soil moisture and underground fluxes. Program also includes a routine for the calculation of snow fall and accumulation, which is not necessary for semi-arid conditions and will be omitted from further discussion.

All processes are performed sequentially during the computation of one time step, at the end of which the computed variables are stored and updated in memory, as seen in Figure 2.3 below.

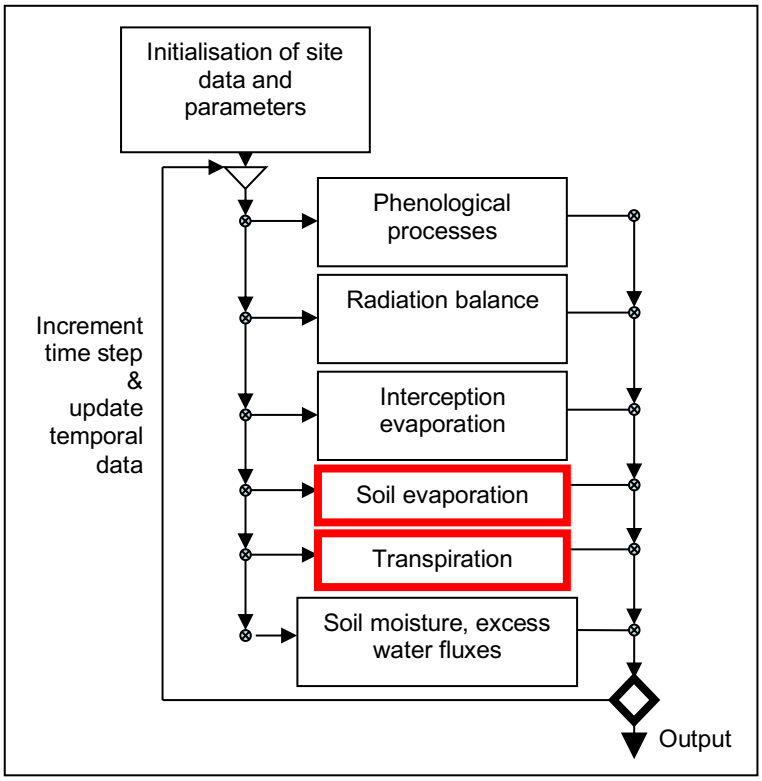

Figure 2-3: process flow for a typical TRAIN simulation in the local mode.

A brief description of the relevant modules is herein given.

Initialisation

According to the land cover classified, the momentum exchange parameters of roughness length and displacement height are defined. Soil and canopy water storage compartments, vegetation cover and surface albedo are given initial values using the input data.

Soil evaporation

Currently not simulated by TRAIN

Transpiration

Transpiration is modelled using the Penman-Monteith equation (eqn. 1.10):

$$\lambda E = \frac{s(R_n - G) + \rho_a c_p D / r_a}{s + \gamma(1 + r_c / r_a)}$$

In order to compute the total canopy resistance for water vapour (r-c) TRAIN uses the following equation:

$$r_c(T, LAI, \theta) = a_0 + a_1 r_c(T) + a_2 r_c(LAI) + a_3 r_c(\theta) \qquad (2.4)$$

With: T air temperature, °C;

LAI leaf area index, dimensionless;

Θ soil moisture deficit, mm

$$r_c(T) = (T + b_1)^4;$$
$$r_c(LAI) = \exp(b_2 LAI);$$
$$r_c(\theta) = (\theta + b_3)^4;$$

Values for the coefficients $a_0 - a_3$ and $b_1 - b_3$ were obtained for this version through calibration using data from a temperate grassland field site in Switzerland (Menzel 1996).

Table 2.1: parameters for equation 2.4 (Menzel 1996)

	a_0	a_1	a_2	a_3	b_1	b_2	b_3	r^2
$LAI \geq 2$	37.52	5.4E-5	2420.5	3.0E-5	4.43	-1.75	-20.51	0.67
$LAI < 2$	-227.3	2.98	487.6	2.5E-5	-	-0.33	-2.05	0.92

The total aerodynamic resistance to water vapour is simulated in TRAIN by the semi-empirical relationship:

$$r_a = 4.72 \frac{\ln^2\left(\frac{z}{z_0}\right)}{1 + 0.54u} \qquad (2.5)$$

With: z height of measurement, m;

z_0 roughness length (height at which extrapolated wind speed equals zero; apparent sink for momentum), m;

u wind speed at the measurement height, $m \cdot s^{-1}$.

2.6.3. limitations of the model

The model TRAIN lacks several crucial components of the eco-hydrological system, namely: soil evaporation, light penetration through the canopy and leaf growth. Nevertheless simple models such as TRAIN enable one to assess, albeit crudely, sensitivity of the eco-hydrological system to changes in key parameters (r-a, for instance) with regards to key processes, such as ecosystem ET.

(3) Results and discussion

(3.1) Seasonal and diurnal dynamics of the important micrometeorological variables used in this study

3.1.1. General

Twenty-four hour data exists for the majority of the variables used in this study for >89% of the period of study (1.1.2003 -31.12.2004). Missing data points are sporadic and clumped in isolated events, due either to maintenance or manual removal. Sensible heat flux, latent heat flux and air temperature, which were used in the inverse approach in this study are discussed herein.

3.1.2. Sensible and Latent Heat fluxes

Sensible (*H*) and latent (*LE*) heat fluxes are given in fig. 3.1, along with the net radiation and ground heat flux. Sensible heat alone comprises on average 76% of the available energy (Rn - G) annually, while latent heat equals ca. 17%. An assessment of the energy balance closure in Yatir Forest has proven to be very high: 99% on average, including canopy heat storage (Agam *et al.*, submitted). Sensible heat flux (*H*) peaks around noontime in January and 14:00 in July, reaching 145 Wm^{-2} and 550 Wm^{-2} in January and July, respectively. Daytime average is 20 Wm^{-2} for January and 178 Wm^{-2} for July. The large outgoing sensible heat flux coincides with the time of hottest air temperature (see fig. 2.1). In the following It will be concluded that DT = Ta – Tskin at summer is low relative to the annual average, despite the high H, suggesting that r-a is lowest during this period.

LE values reach an average daily maximum of 72 Wm^{-2} and 50 Wm^{-2} in January and July, respectively. The *evaporative fraction* α = LE/(LE + H) varies accordingly, averaging 57% in January and 6% in July (1/2 hr basis). LE is easily transformed to evapotranspiration, *ET*, through the division by the latent heat of vaporisation, λ, which is a weak function of temperature, *T*:

$$ET = LE/\lambda(T) \qquad (3.1)$$

Although the atmospheric demand for ET is highest in June-August, LE peaks during March, when the atmospheric demand is milder; it follows that the total resistance to water exchange is very high during June-August, restraining the flow from potentially high values.

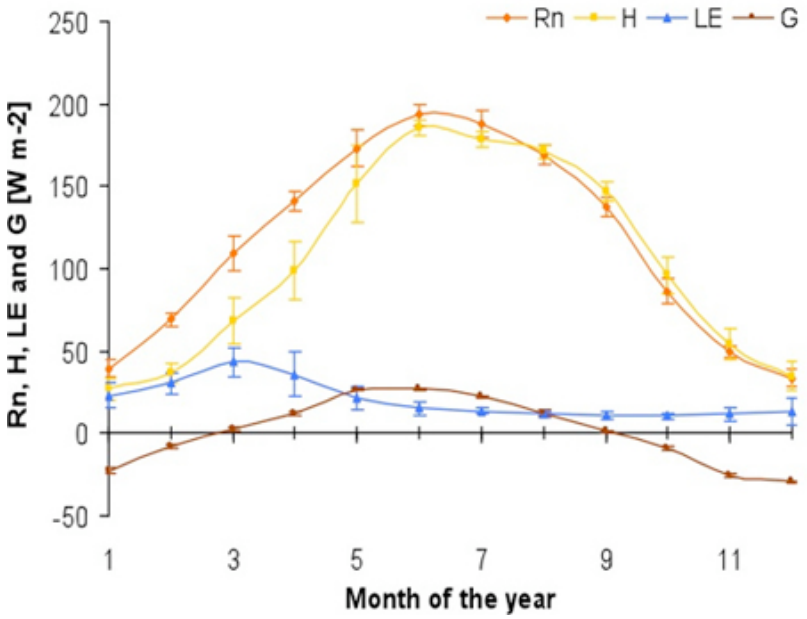

Figure 3-1: multi-year average cycle of the fluxes of: net above canopy radiation, *Rn*, sensible heat, *H*, latent heat, *LE* and ground heat, *G*. sensible heat is the dominant outgoing heat flux throughout most of the year (March-December), comprising 75-95% of the available energy, *A* = *Rn*-*G*. Latent heat peaks in March.

3.1.3. Air temperature

Air temperature follows the incoming global radiation, lagging 1-2 hrs (data not shown). Of all the temperature readings, the temperature at 19m varies diurnally the least, with 4°C maximum daily difference in January and 10.6°C in July. The vertical temperature profile, sketched for three different times of day (figs 3-2a-b), reveals that air temperature increases descending from 19m to 5m and then declines from 5m to 1m. Air temperature descending below 1m to the ground is assumed to increase, although not directly measured. The air column is unstable throughout most of the day due to the creation of buoyant air parcels throughout the canopy air column. This is evident from the strongly negative vertical air temperature gradients at noontime (ca. -0.1°Cm^{-1} in January and -0.6°Cm^{-1} in July) and a weakly positive gradient later in the day (at 20:00).

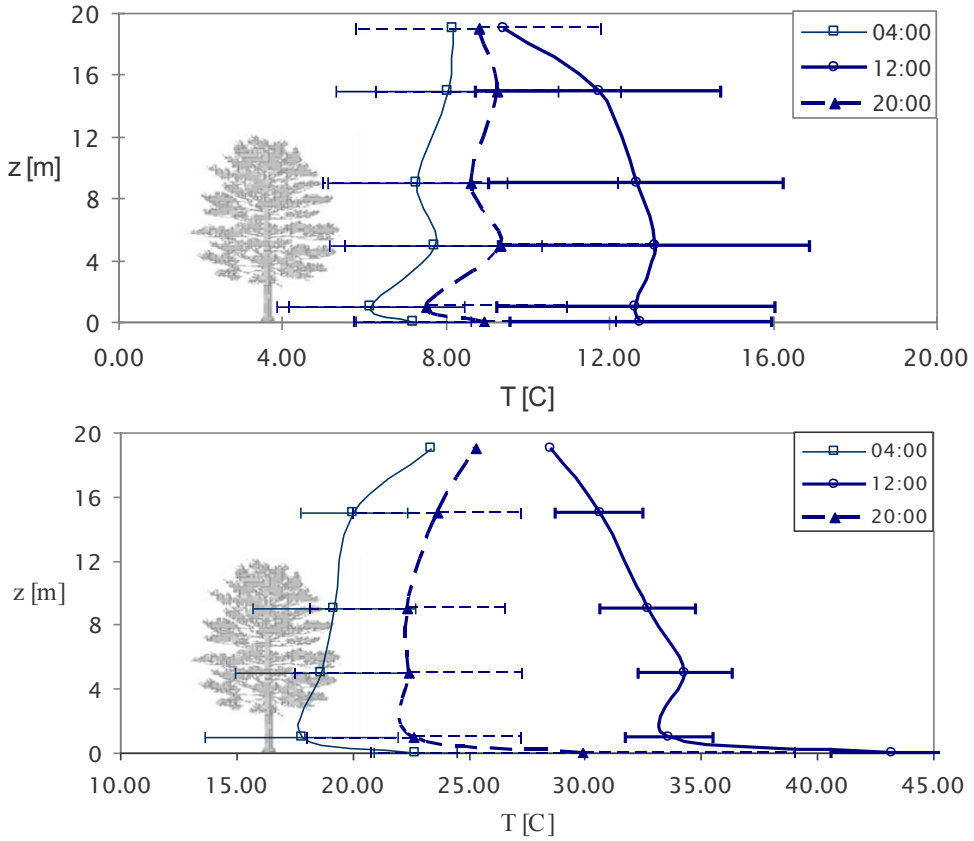

Figure 3-2a-b: profiles of the air column temperature as measured adjacent to the eddy flux tower averaged monthly for: (a) January 2004; (b) July 2004. Profiles of 04:00, 12:00 and 20:00 are presented. Air temperature gradients are less than the gradient of neutral stability during daytime leading to instability of the air column throughout the day.

(3.2) Forest & ground 'skin temperature'

Skin temperature of the forest was estimated in two different ways successively during the study.

3.2.1. Simple grey body temperature

Skin temperature was first estimated as simply the grey-body temperature of upwelling long-wave radiation, obtained from a single LWR sensor, the PIR3, which is situated above canopy level, as in fig. 3.3 below, using equation 3.2, which is the inverse form of the Stefan-Boltzmann equation (eqn. 2.3):

$$T_{skin} = \sqrt[4]{\frac{L_{top\uparrow}}{\varepsilon\sigma}} \qquad (3.2)$$

This temperature was termed $T_{1STREAM}$ since it is obtained from observations of a single sensor. Diurnal trend of $T_{1STREAM}$ for a typical day in January (and another for July) is presented in figs 3.6a-b below. Daily minimum-maximum temperature span was 6.3°C for $T_{1STREAM}$ in January and 17.3°C in July. The corresponding temperature ranges for T(19m) were lower: 3.4°C in January and 10.6°C in July. After sundown $T_{1STREAM}$ decreased below T(19m) corresponding to a negative temperature gradient of up to 1.4°C. Average daily minimum and maximum were 9-15°C for January and 21-39°C for July (2004 data).

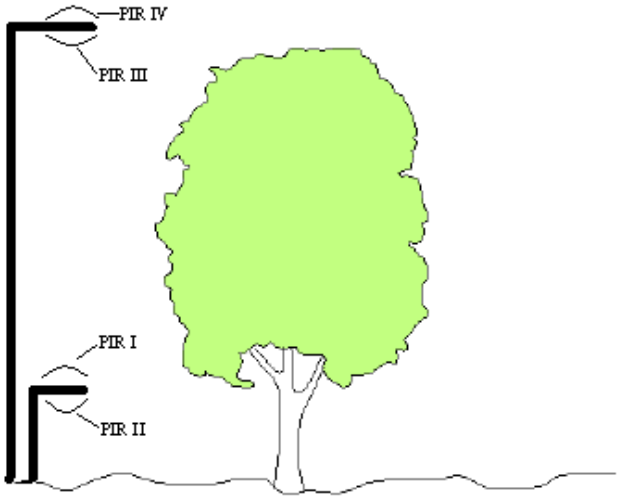

Figure 3-3: long-wave radiation sensor array at the forest research site. Forest 'skin' temperature was obtained in either of two methods: (a) using PIR3 data only (the $T_{1STREAM}$ method); (b) using data from sensors PIR1 - PIR3 (the $T_{3STREAM}$ method).

3.2.2. Detailed radiometric temperature ($T_{3STREAM}$)

To assess the usefulness of the simple radiometric method ($T_{1STREAM}$), a second, more detailed assessment of the skin temperature was performed. Balance equations were written for the long-wave radiation above and below canopy level from which temperature of the top soil and canopy were separately inferred. The radiative forest skin temperature (dubbed $T_{3STREAM}$ for three-stream radiative temperature) was calculated from the weighting of soil and canopy temperatures based on their surface areas, neglecting differences in heat diffusivity and specific heat of the canopy and air. The balance equations and summation of temperatures are presented:

a) For soil temperature:

LWR_bottom_up = emitted by soil + reflected by soil :

$$L_{bot\uparrow} = \varepsilon_s \sigma T_s^4 + (1-\varepsilon_s) L_{bot\downarrow} \tag{3.3}$$

b) For top of canopy:

LWR_top_up = total up from canopy + total up from below canopy :

$$L_{top\uparrow} = f_c L_{c\uparrow} + (1-f_c) L_{bot\uparrow} \tag{3.4}$$

c) For canopy bottom:

LWR_bottom_down = total down from canopy + total down from sky :

$$L_{bot\downarrow} = f_c L_{c\downarrow} + (1-f_c) L_{top\downarrow} \tag{3.5}$$

A schematic that represents the T3STREAM derivation is given in fig. 3.5.

The canopy fraction, *fc*, was taken as equal to the midday summer shaded fraction of ground, SF, as was computed by (Raz Yaseef, 2008). Ground and canopy emissivities were estimated as **0.94** and **0.99**, based on values in (Rees, 2001); a large uncertainty was associated with these values because of the lack of site specific data and a wide range in the literature.

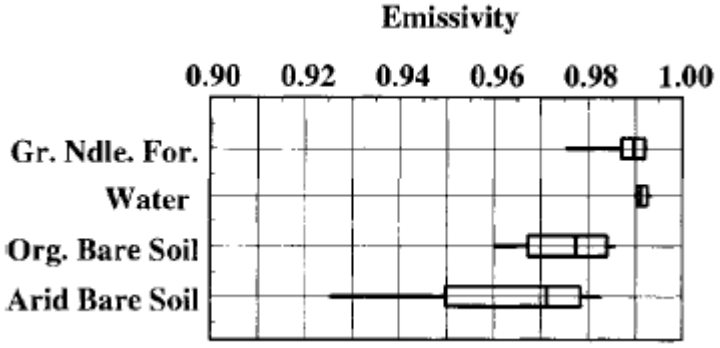

Figure 3-4: box plots of classification-based emissivity ranges in the 10.8- 11.3 μm thermal infrared band based on model predictions and measurements. Four classes of land-cover are presented: green needle forest, water, organic bare soil and arid bare soil. Box shows the 16-84 percentiles and mean. After Snyder et al, 1998.

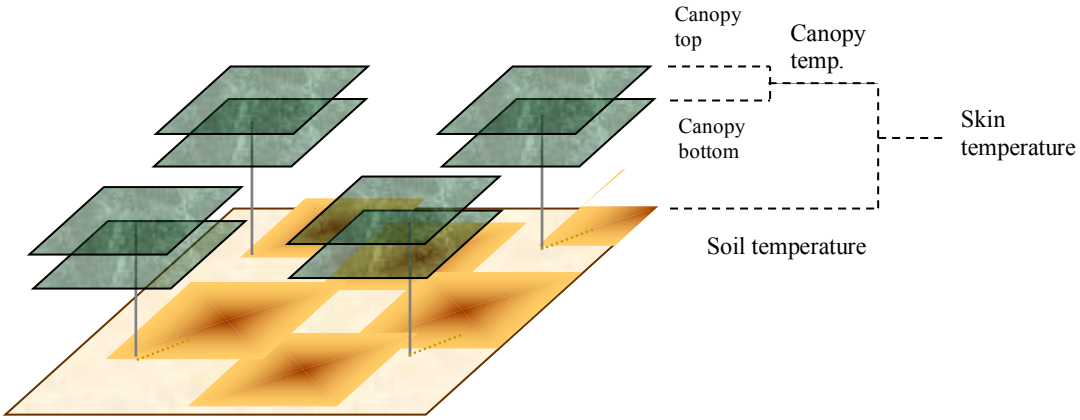

Figure 3-5: Schematic of the forest canopy emphasizing the three layers given by the radiative temperature assessment $T_{3STREAM}$. The concealment of the bottom canopy foliage is responsible for important deviations of $T_{1STREAM}$ from the true skin temperature.

The resulting surface temperatures were estimated as:

Soil temperature: $$T_s = \left(\frac{L_{bot\uparrow} + (1-\varepsilon_s) L_{bot\downarrow}}{\varepsilon_s \sigma} \right)^{1/4} \qquad (3.6)$$

Canopy top and bottom temperatures were lumped into a single approximation:

$$T_c = \sqrt[4]{\frac{L_c}{\varepsilon_c \sigma}} \qquad (3.7),$$

With: $L_c = a \cdot L_c\downarrow + (1-a) \cdot L_c\uparrow$, where a is a weighting parameter, which was estimated as 0.5 in all following calculations. Summation of these temperatures to give the total skin temperature was as follows:

$$T_{3STREAM} = \frac{1 \cdot T_s + LAI \cdot T_c}{1 + LAI} \qquad (3.8)$$

Average Diurnal course of $T_{3STREAM}$ and $T_{1STREAM}$ are given in figures 3-6a-b below. The range of values due to emissivity uncertainty for the 1-stream method is almost twice that for the 3-stream method. The daily minimum-maximum temperature span is 7.0°C for $T_{3STREAM}$ in January and 19.2°C in July, considerably larger than those for $T_{1STREAM}$. Average daily minimum and maximum $T_{3STREAM}$ are 8-15°C for January and 20-40°C for July (2004 data).

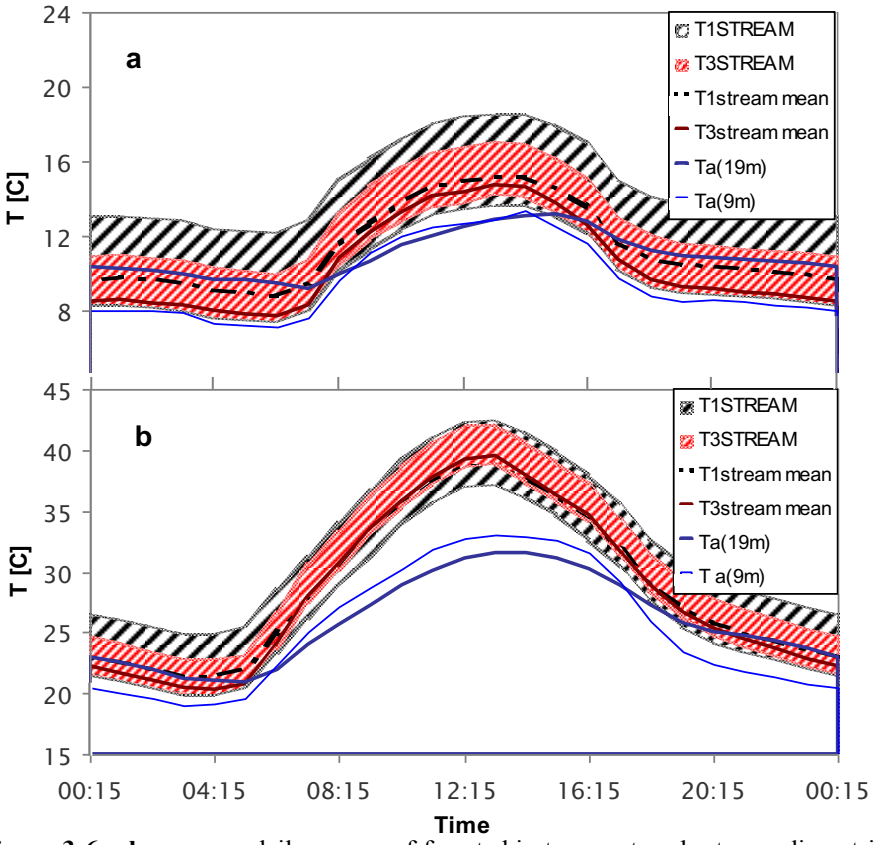

Figure 3-6 a-b: average daily course of forest skin temperature by two radiometric methods: $T_{1STREAM}$, derived from a single LWR sensor, and $T_{3STREAM}$, derived from a radiation balance using three LWR sensors, showing a large uncertainty due to long-wave emissivity. Also shown are air temperature at the reference point above canopy (T_A19) and temperature of air at canopy level (T_A9). Data is for (a) January 2004; (b) July 2004.

3.2.3. Comparing the temperature assessments

Overall, the two methods give quite similar temperatures (using mean emissivities), but significant differences give rise to a significant difference in the magnitude of T_A-Tskin causing a difference in r-a by the inverse method. Both $T_{1STREAM}$ and $T_{3STREAM}$ temperatures are characteristically hotter than the air within the canopy day and night: $T_{1STREAM}$ by 1.5-2.3°C throughout the day whereas $T_{3STREAM}$ by 0.8-3°C (January data). Both $T_{1STREAM}$ and $T_{3STREAM}$ temperatures are hotter than air temperature at the reference point (19m) during daytime: noon-time T(19m)-$T_{1STREAM}$ is -2.5°C in January and -7.5°C in July. Corresponding values for T(19m)-$T_{3STREAM}$ are -1.8°C in January and -8.2°C in July. The most significant difference between the two estimates is by night: $T_{1STREAM}$ is hotter than $T_{3STREAM}$ by more than 1.0°C in January and July.

The range of uncertainty in the components of canopy emissivity is much smaller than the overall emissivity uncertainty – a fact which is reflected in the temperature uncertainty. The canopy contributes largely (ca. 2/3) to the total skin temperature in T3stream; this may explain the smaller uncertainty range of temperature due to emissivity in T3stream, seen in fig. 3-6a-b.

T1stream is the simpler method; we would expect it to be less sensitive to minute variations and possibly overestimate overall temperature.

(3.3) Estimating r_a by the inverse method

3.3.1. Assessing the inverse method

A need arose to determine if DT as measured can explain the measured heat flux using eqn. 2.1. Four different methods for the calculation of DT were considered. These are:

(1) $DT = T_A - T_{AIR\text{-}C}$;

(2) $DT = T_A - T_{1STREAM}$;

(4) $DT = T_A - T_{COMPOUND}$;

(3) $DT = T_A - T_{3STREAM}$.

With: T_A air temperature at 19m above ground level;

$T_{AIR\text{-}C}$ average of the air temperatures at 1, 5 and 9m above ground level;

$T_{COMPOUND} = (T_{1STREAM} + T_{AIR\text{-}C})/2$ average of $T_{1STREAM}$ and $T_{AIR\text{-}C}$.

Half hour values of H were plotted against corresponding DT values for July 2003, Jan 2004 and July 2004. The data was screened for friction velocity higher than a certain threshold due to unreliable eddy covariance measures during low u* (Rotenberg E, per. com.). A linear regression curve was drawn for each plot, thus giving intercept and slope values, $s = -\rho C_p/r\text{-}a$, by which to assess the relationship. Table 3.1 below gives slope, intercept and r^2 values for all 7 tests performed.

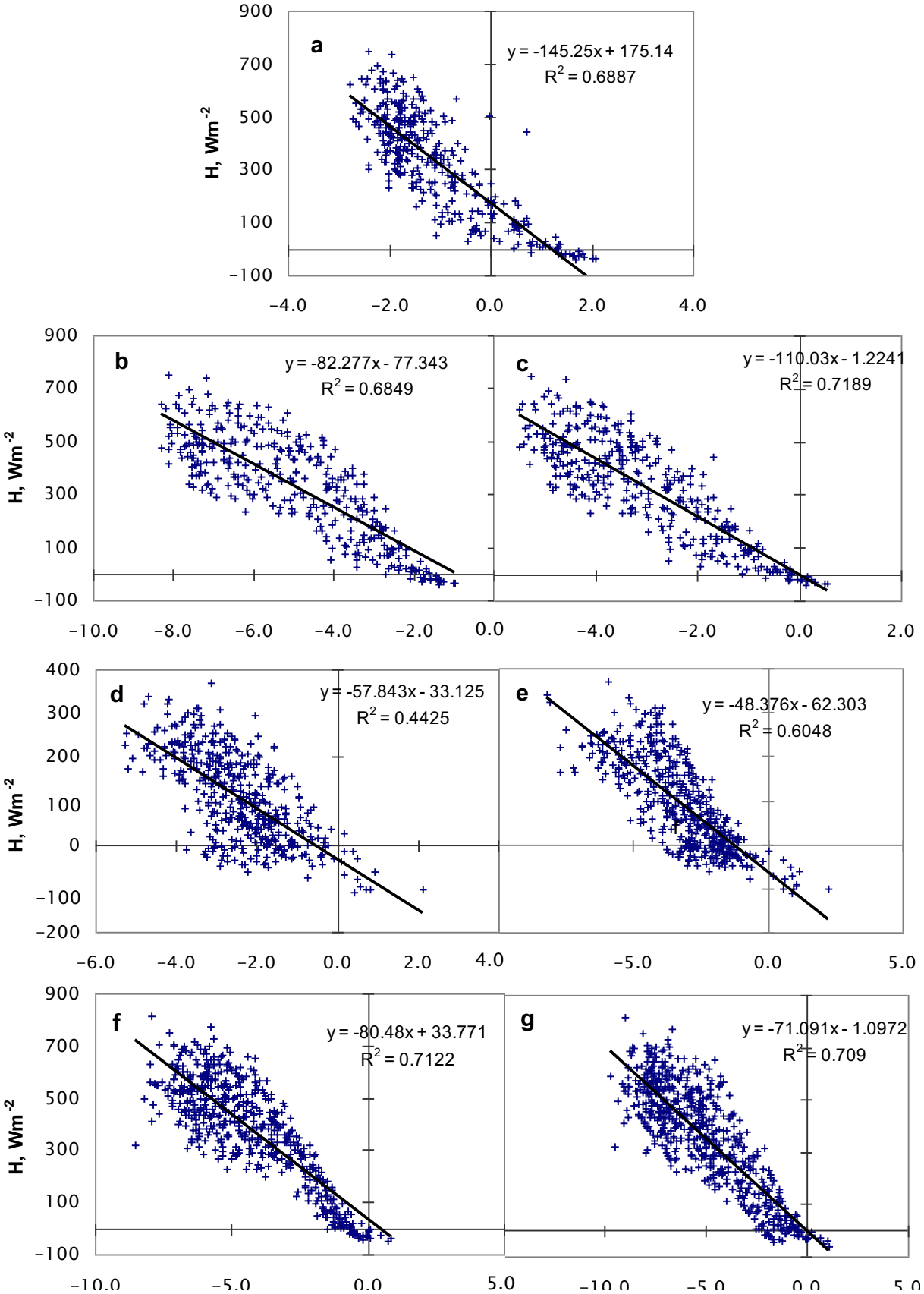

Figure 3-7(a-g): (a) H vs. DT measured as T_A - T_{AIR-C}; (b) H vs. DT measured as T_A - $T_{1STREAM}$; (c) H vs. DT measured as T_A - $T_{COMPOUND}$; (d) H vs. DT measured as T_A - $T_{1STREAM}$; (e) H vs. DT measured as T_A – $T_{3STREAM}$. (f) H vs. DT measured as T_A - $T_{1STREAM}$. (g) H vs.

DT measured as $T_A - T_{3STREAM}$. T_A = T19m, unless otherwise mentioned. Data of a -c is for **July 2003**, n = 368; data of d, e is for **January 2004**; Data in f, g is for **July 2004.**

According to eqn. 2.1 the plot of H vs. ΔT going through the origin should produce a line with a slope of $-\rho C_p/r\text{-}a$. Both ρ and C_p are weak functions of temperature and their product is nearly constant at the range of ambient temperature (+/-5%); therefore it was expected that variations in the slope of the curve would predominantly reflect variations in monthly average r-a, which could then be estimated.

Table 3-1: regression coefficients for H vs. DT tests

	Correlation	Period	r^2	Slope, $Wm^{-2}K^{-1}$	Average r-a, sm^{-1}	Intercept, Wm^{-2}
a	**DT = T(19m) $-T_{AIR\text{-}C}$**	Jul 2003	0.69	-145	8	175
b	**DT = T(19m) $- T_{1STREAM}$**	Jul 2003	0.68	-82	15	-77
c	**DT = T(19m) $-T_{COMPOUND}$**	Jul 2003	0.72	-110	11	-1
d	**DT = T(19m) $- T_{1STREAM}$**	Jan 2004	0.44	-58	21	-33
e		Jul 2004	0.71	-80	15	34
f	**DT = T(19m) $- T_{3STREAM}$**	Jan 2004	0.60	-48	25	-62
g		Jul 2004	0.71	-71	17	-1

All H vs. ΔT plots appeared to be linear – narrowly scattered along a line, with the majority of points concentrated to one side. Linear regression yielded intermediate regression coefficients ($p < 0.00001$), in support of the expected relationships between H and ΔT, which also indicate intercept near zero. In general, data of January show poorer linear correlation between H and ΔT as measured by either method used ($0.44 < r^2 < 0.6$). Correlation coefficients using $T_{1STREAM}$ varied widely across years, with two very different intercept values, suggesting a strong sensitivity to variations in the data.

According to theory, $H(\Delta T=0)=0$; or in other words, there should be no statistically significant intercept to the regression line. Dataset A (table above), with a positive intercept of 175 Wm^{-2}, seemed to overestimate H for a given ΔT; dataset B, with a negative intercept of 77 Wm^{-2}, seemed to underestimate H. The correlation datasets with the smallest intercept, and therefore best fit to

theory, were set C (where T is a combination of average canopy air temperature and $T_{1STREAM}$, fig. 3-7c) and set G (using $T_{3STREAM}$, Fig. 3-7g).

The good correlation between H and ΔT of set C suggests that T1stream is an overestimation of the true skin temperature, and that the temperature of canopy elements hidden by the uppermost foliage plays an important role. Figure 3.8, in which canopy air temperature is shown along with T1stream and T3stream, reinforces this view as it can be seen that the more detailed $T_{3STREAM}$ more closely follows the temperature of the canopy air than T1stream.

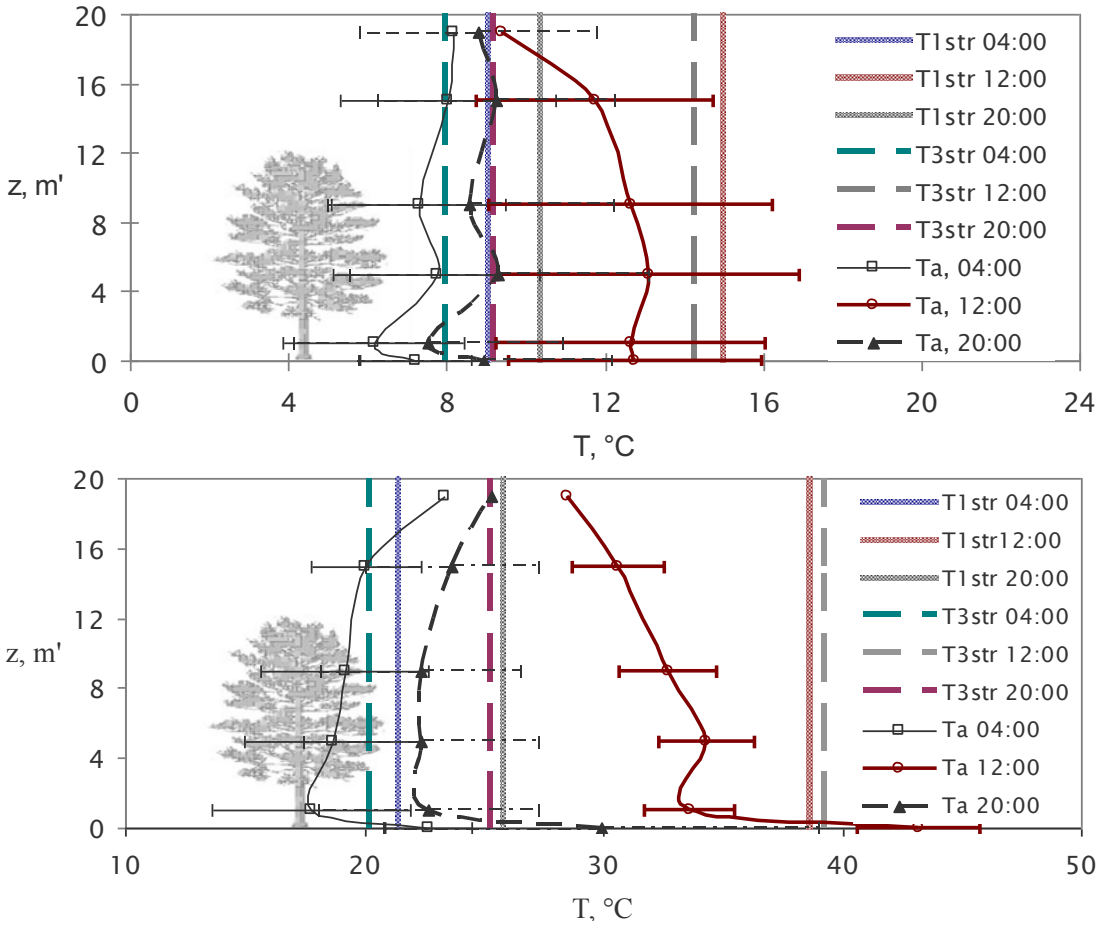

Figure 3-8: $T_{1STREAM}$ and $T_{3STREAM}$ monthly average for three hours of the day: 04AM, 12PM, 8PM for (a) January and (b) July of 2004 plotted with air temperature profiles. T1stream is hotter than the air temperature in all cases. T3stream estimates lie almost always between their corresponding T1stream estimate and the air profile temperature,

3.3.2. **Aerodynamic resistance timeseries**

½ hourly values of aerodynamic resistance were obtained using the inverse method (eqn. 2.2). These values were then screened for daylight hours and averaged over the day to give daily averaged daylight hour (D.A.D.H) values (due to low quality of H values measured at night by the EC method, night-

time values were notably unrealistic, often with negative values). Figure 3.9 below shows inter-seasonal as well as intra-seasonal differences between DADH values using the three different methods ($T_{1STREAM}$, $T_{3STREAM}$ or TRAIN – eqn. 2.5).

A distinct seasonality can be seen in r-a estimated by the inverse approach, that is not seen in TRAIN. Table 3.2 below shows the seasonal and annual differences.

The seasonality in r-a is attributable to the intensity of turbulence in the canopy, reflected by the changes in atmospheric stability revealed earlier in this text. In its current form, TRAIN does not include stability considerations.

Table 3-2: r-a values computed either by TRAIN or by the inverse method; averaged monthly / annually

Series	TRAIN, sm^{-1}	Inverse (T_{comp}), sm^{-1}	Inverse (T_{3STR}), sm^{-1}
Max. monthly avg.	19	28	26
Min. monthly avg.	16	10	11
Annual	17	18	20

A notable difference lies between the two inverse method estimates. Inverse ($T_{3STREAM}$) values for Jul 2003 were more than double those of Inverse (Tcomp).

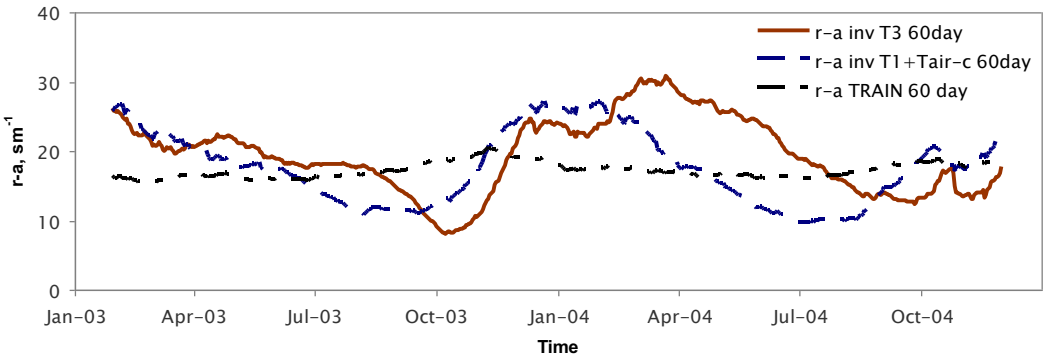

Figure 3-9: moving averages of aerodynamic resistance calculated using different skin/ screen temperature estimates: (1) Tskin calculated as $T_{1STREAM}$ and T_{AIR-C} compounded; (2) Tskin calculated using $T_{3STREAM}$; (3) using TRAIN. TRAIN data exhibit least inter-season variation, whereas inverse method exhibits high inter-season (delta~10s/m) as well as seasonal variability. r-a inv T3 is often twice the values of r-a inv, on a diurnal to monthly basis.

(3.4) Sensitivity of ecosystem evapotranspiration to aerodynamic resistance

3.4.1. Estimating the sensitivity of ET to changes in aerodynamic resistance

In order to fully estimate the sensitivity of ET to changes in the aerodynamic resistance, it is required to simulate ET with accurate resistance values for the period of several days to a year. A preliminary experiment was performed to indicate the magnitude and direction of the sensitivity. A typical 'baseline' set of values of net radiation, ground heat flux, air temperature, VPD, aerodynamic and canopy resistances was conceived for the experiment using the average noontime values for the above variables for 2003. Using the Penman-Monteith equation (eqn. 1.1), ET was calculated for the baseline value set and for 5 additional sets, each created by arbitrarily perturbing a single variable of the baseline by 50% or 11°C. The deviation of ET from the baseline ET was then calculated; values are given in table 3.3.

Table 3-3: 'Baseline' and 'perturbed' values for ET sensitivity test: year-round average noontime data used.

	T_A, °C	D, kPa	Rn, Wm^{-2}	G, Wm^{-2}	r-a, ms^{-1}	r-c, ms^{-1}
Baseline	22	1.9	500	57	22	160
Perturbation	33	2.9	750	85	33	240

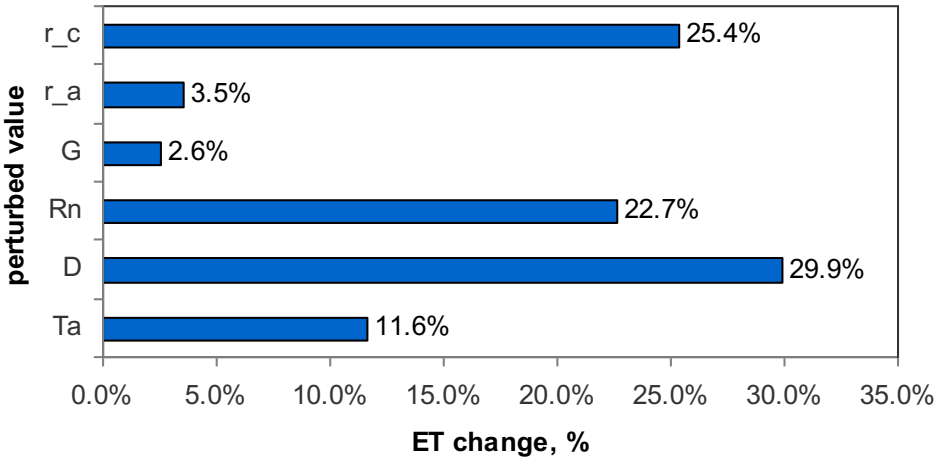

Figure 3-10: changes in evapotranspiration (ET) brought about by arbitrarily perturbing either one of the following variables: r-c, r-a, G, Rn, VPD and Ta by 50% /11°C from mean annual noontime values. r-a is shown to have a minor direct effect. VPD has the highest direct effect.

In this simple experiment several gross oversimplifications are inherent (e.g. the increase of temperature was allowed without due modulation of the net

radiation balance) resulting in the highly suspicious result of an increase in ET with an increase in r-a. The sign of the effects was therefore ignored.

The experiment showed that when isolated, the sensitivity of ET to perturbations in the parameters indicated ranged between 5 and 30 %, with r-a having the smallest impact at approx. 5%. During the course of a season, actual r-a in Yatir may increase as much as two-fold, leading to a significant change in ET.

3.4.2. Simulating ET with TRAIN

Simulations of ET were performed using a somewhat modified version of TRAIN which allowed for manual provision of r-a timeseries as input. The model was run for the entire study period (2003-2004) several times, using either internally calculated r-a or the r-a calculated by the inverse method. Predetermined leaf area index and intercept storage capacity data files, specifically developed for simulation of Yatir Forest were used as input (Hausinger 2009).

Table 3-4: initiation parameters for the model runs

Parameter	Value	Parameter	Value
Site elevation (m)	650	Soil depth (mm)	1300
Wind speed, air temperature and RH measurement height (m)	15	Initial soil moisture (mm)	500
Soil type	Loamy	Field capacity (mm)	588
Land-cover type	Conifer forest	Permanent wilting point (mm)	182
Time step	day	Irrigation (Y/N)	No

A comparison of ET simulated by TRAIN and ET measured by the EC method is presented in figure 3.12 below. An overall good agreement appears between measured ET and the model simulation; nevertheless, the similarity is only apparent, as major hydrological processes and energy components were not incorporated into the model; also, assumptions regarding soil moisture and LAI were subject to arbitrary choice.

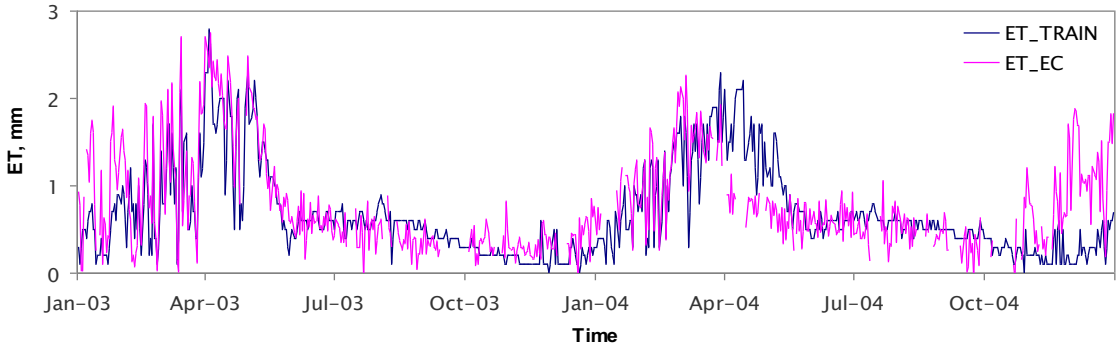

Figure 3-11: ET as measured by the EC method along with corresponding ET simulated by TRAIN. Data is for 2003 – 2004.

As can be seen in table 3.6 below, running TRAIN with the internally calculated r-a (eqn. 2.5) resulted with a total ET of 253mm for the hydrological year 2003/4. When run using r-a calculated by the inverse method, TRAIN gave ET values lower by 13-25% than the original TRAIN run.

Table 3-5: evapotranspiration, measured by the eddy-covariance method vs. simulated in TRAIN. Gap-filled value of ET from EC method: Raz Yaseef (2009). H.y.=hydrological year

ET source	cumulative ET, 2003/4 *H.y.*, mm	relative to ET from EC	relative to ET of ordinary TRAIN
From eddy covariance (EC)	232	100%	92%
using r-a TRAIN	253	109%	100%
using r-a inv T3str	220	95%	87%
using r-a inv Tcomp	189	81%	75%

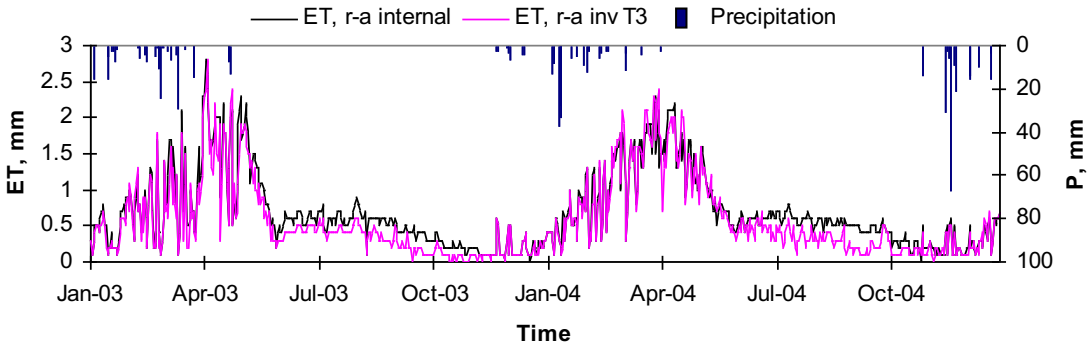

Figure 3-12: Evapotranspiration simulated by TRAIN using two different r-a timeseries: r-a calculated internally by the program ('r-a internal'), and r-a calculated by the inverse method using $T_{3STREAM}$ as skin temperature. Differences are mostly evident during the dry season (JUN-OCT), when the incoming energy is the highest and the energy partitioning between sensible heat and latent heat is strongly dependent on the aerodynamic resistance, according to the Penman Monteith formula.

Looking in figure 3.13, differences in ET between runs using different r-a estimates are most evident during the dry season (Jun-Oct), when the incoming energy is the highest. This could be attributable to the nature of the Penman Monteith formula.

3.4.3. comparing aerodynamic resistances of Yatir Forest with other ecosystems

Forests are often characterised by lower r-a values owing to their larger roughness length, which acts to increase the turbulence in the air column above the vegetation. The roughness length has been parameterised for various land uses including field crops and natural vegetation, and is generally considered a function of the vegetation height for dense homogenous canopies. Forests, especially coniferous (e.g. pine forests) are difficult to model because of the combined effects of bluff-body roughness produced by the tree trunk and branches and the effects of 'porous' roughness elements (Thom, 1972). Following Lettau (1969), (Shaw & Pereira, 1982) used a numerical model to show a relationship between roughness length (z_0), plant height (h) and canopy density (represented by Plant Area Index – PAI). They based their estimate on numerically solving the flow equations in 1-D over an idealised plant profile assuming spatial horizontal homogeneity. They show that at low plant area to ground area ratios, z_0 increases with increasing density, and the roughest surfaces were those in which plant material was skewed towards the top of the canopy, indicating that when the vegetation is relatively sparse, the greatest drag is achieved when plant material is projected to the upper part of the canopy.

Assuming that the height of the vegetation outside of the forest is on the order of 1 meter and the plants are cushion-like in appearance (typical for dry-land vegetation) with z_max/h ~ 0.2, and a PAI of far less than one, the roughness length (according to fig. 3-13) is 6 – 14 cm. In comparison, a roughness length for the forest is ca. 1.2m. It is plausible that differences between instabilities within the forest and outside the forest take place, as they are induced by thermal gradients and free convection. Nevertheless it would be safe at this point to assume that these differences do not contribute much to the difference in r-a and that r-a of the two ecosystems can be compared based on roughness

length, displacement height using eqn. 1.2 assuming neutral stability (summarised in table 3.6).

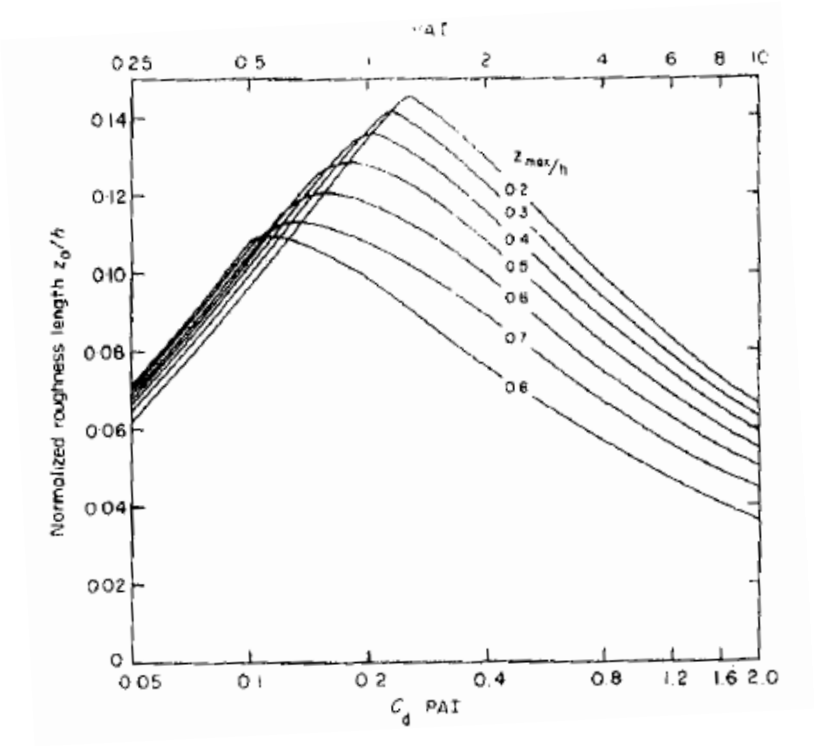

Figure 3-13: normalised roughness length as a function of C_d*PAI (C_d is coefficient of drag, ca. 0.2 here). Curves are labelled according to the height at which density reaches a maximum. From Shaw and Pereira (1982).

Although not directly applicable to sparsely planted pine forests, the data in table 3.6 shows differences between ideal homogenous tall stands (12m') and low, sparse shrubland. From the data it can be approximated that the ratio of aerodynamic resistances is on the order of 2/7 for the forest, or a 71% reduction.

Table 3-6: aerodynamic resistance in Yatir Forest and outside it using annual noontime wind

	Shrubland	Forest	reduction
A. Resistance, *normalised*	1	0.29	71%

From this preliminary yet robust comparison it follows that Yatir Forest significantly changes the aerodynamic resistance and flow regime relative to its surroundings, therefore aiding in heat dissipation into the air above it.

(4) Conclusions

The overall resistance to mass transfer between foliage and the atmosphere is a key component in the control of heat, water and trace gas exchange at the land-air interface. Long-term micrometeorological data from the semi-arid forest of Yatir in Israel were analysed to obtain an estimate of the forest 'skin' temperature representing a combination of canopy and soil temperatures in this open canopy forest. The total aerodynamic resistance to heat and water vapour transport was calculated using the aforementioned temperature measurements. Aerodynamic resistance was low relative to other Mediterranean forest environments, with an annual average of 19 sm^{-1} and yearly minimum of 10 sm^{-1}. Model simulations of forest Evapotranspiration (ET) varied by up to 25% as a result of using different estimates of aerodynamic resistance.

Our data-based estimates of r-a are among the lowest reported for forests of the FLUXNET network, which are mostly temperate to dry-sub humid forests, and help explain the unusually large sensible heat flux (up to 550 Wm-2) observed in this system, and which is critical for heat dissipation in dry ecosystems such as Yatir, where the "conventional" cooling by water evaporation (latent heat flux) is greatly suppressed (less than 6% of the total incoming energy in July).

Aerodynamic resistance using the inverse method based on actual measurements showed a distinct seasonality that was not captured by the TRAIN model, which uses a simple empirical relationship between aerodynamic resistance and wind speed and was developed in temperate conditions.

Using two different approaches for the assessment of skin temperature, two datasets of aerodynamic resistance were developed. Both datasets were developed from actual measurements and show a distinct seasonality. It remains to conclude which method assesses better the true aerodynamic resistance in Yatir Forest.

The planting of Yatir Forest increased the total heat dissipation rate of its semi-arid environment, by lowering the aerodynamic resistance to heat by an estimated 71%

relative to its surroundings, aiding to relieve the heat load of the forest and help explain its unexpectedly high productivity under the local harsh environmental conditions.

Appendix A: gap-filling protocols

1. Gap filling protocol one (GF–1):

   Standard time unit: day

   Gaps of 3 days or shorter: fill using linear interpolation

   Gaps longer than 3 days: fill using surrogate good quality data as follows:

   $$x_i = y_i - (y_0 - x_0) \qquad \text{(A00.1)}$$

   With: x_i data point i in gap-laden series x;

   y_i data-point i in surrogate data series y;

   y_0 y-series data-point preceding gap;

   x_0 data-point preceding gap in series x.

   Example:

   Series x: 1 2 23 __ __ 465 25 …

   Series y: 1 3 17 15 100 444 22 …

   X4 = y4 – (y3 – x3) = 15 – (17 – 23) = 21

   X5 = y5 – (y3 – x3) = 100 – (17 – 23) = 106

2. Matlab script 'gap_one.m'

```
function [data2]=gap_one(data)
% Function for gap-filling a vector (sequence) of patchy data
% DESCRIPTION
% Looks for file 'data' in the workspace and returns a gap-filled version of it.
% Gap-filling is done by linear interpolation.
% Written by Amir Tal
% Version: 2.0  Date:Thursday September 10 2009
% WARNING: data variable must exist in the workspace. data must be a
% COLUMN vector.
k=1; % initiation

v1=find(isnan(data)); % getting the gap indices

v2(1)=v1(1); % the  start of the first gap

% loop that looks for gaps in the 'v1' sequence and "collects" information on them
for i=2:(length(v1)-1)
```

```
    if v1(i)~=v1(i-1)+1
        v3(k)=v1(i-1);
        v2(k+1)=v1(i);
        k=k+1;
    end
end
v3(k)=v1(end);
v3=v3';
v2=v2';
space_within=zeros(k,1);
% clearance_before=zeros(k-1);
space_within(:)=v3(:) - v2(:)+ones(k,1); % getting the length of gaps
% clearance_before(2:k-1)=v2(2:end) - v3(1:end-1); % getting the clearance before gaps
data2=data; % defining the output variable

% checking for the location of the first gap
y2=data(v3(1)+1);
if v2(1)==1
    y1=data(v3(1)+1);
else
    y1=data(v2(1)-1);
end
patch=linspace(y1,y2,space_within(1)+2)';
data2(v2(1):v3(1))=patch(2:end-1);

% closing the gaps
for i=2:k-1
    y1=data(v2(i)-1);
    y2=data(v3(i)+1);
    patch=linspace(y1,y2,space_within(i)+2)';
    data2(v2(i):v3(i))=patch(2:end-1);
end

% checking for the location of the last gap
y1=data(v2(k)-1);
if v3(k)==length(data)
    y2=y1;
else
    y2=data(v3(k)+1);
end
patch=linspace(y1,y2,space_within(k)+2)';
data2(v2(k):v3(k))=patch(2:end-1);
```

References

Agam, N., Raz Yaseef, N., Rotenberg, E., & Yakir, D. (submitted) Energy balance of a semi-arid forest: assessment of the contribution of soil and canopy heat storage.

Campbell, G.S. & Norman, J.M. (1998) *Introduction to environmental biophysics* Springer-Verlag, New York.

Charlson, R.J., Lovelock, J.E., Andreae, M.O., & Warren, S.G. (1987) Oceanic phytoplankton, atmospheric sulphur, cloud albedo and climate. *Nature*, **326**, 655-661.

Charney, J., Quirk, W.J., Chow, S.-h., & Kornfield, J. (1977) A Comparative Study of the Effects of Albedo Change on Drought in Semi-Arid Regions. *Journal of the Atmospheric Sciences*, 1366-1385.

Charney, J.G. (1975) Dynamics of deserts and drought in the Sahel. *Quarterly journal of the Royal Meteorological Society*, **101**, 193-202.

Daamen, C.C. & McNaughton, K.G. (2000) Modeling Energy Fluxes from Sparse Canopies and Understorys. *Agron J*, **92**, 837-847.

Dolman, A.J., van der Molen, M.K., ter Maat, H.W., & Hutjes, R.W.A. (2004). The effects of forests on mesoscale atmospheric processes. In *Forests at the land-atmosphere interface* (eds M. Mencuccini, J. Grace, J. Moncrieff & K.G. McNaughton). CABI Publishing.

Grunzweig, J.M., Gelfand, I., Fried, Y., & Yakir, D. (2007) Biogeochemical factors contributing to enhanced carbon storage following afforestation of a semi-arid shrubland. *Biogeosciences J1 - BG*, **4**, 891-904.

Grunzweig, J.M., Lin, T., Rotenberg, E., Schwartz, A., & Yakir, D. (2003) Carbon sequestration in arid-land forest. *Global Change Biology*, **9**, 791-799.

Howell, T.A. & Evett, S.R. (2004) The Penman-Monteith method. In Section 3 in Evapotranspiration: Determination of Consumptive Use in Water Rights Proceedings, Denver, CO.

IPCC (2001) *Climate Change 2001: The Scientific Basis. Contribution of working group I to the Third Assessment Report of the Intergovernmental Panel on Climate Change* Cambridge University Press, Cambridge.

Jarvis, P.G. (1976) The interpretation of the variations in leaf water potential and stomatal conductance found in canopies in the field. *Philosophical Transactions of the Royal Society of London. B, Biological Sciences*, 593-610.

Lindroth, A. (1993) Aerodynamic and canopy resistance of short-rotation forest in relation to leaf area index and climate. *Boundary-Layer Meteorology*, **66**, 265-279.

Maseyk, K. (2006) Ecophysiological and phenological aspects of *Pinus halepensis* in an arid-Mediterranean environment. Ph. D., Weizmann Institute of Science, Rehovot.

Maseyk, K.S., Lin, T., Rotenberg, E., Grunzweig, J.M., Schwartz, A., & Yakir, D. (2008) Physiology-phenology interactions in a productive semi-arid pine forest. *New Phytologist*, **178**, 603-616.

Menzel, L. (1996) Modelling canopy resistances and transpiration of grassland. *Physics and Chemistry of The Earth*, **21**, 123-129.

Monin & Obukhov (1954) Basic laws of turbulent mixing in the surface layer of the atmosphere. *Tr. Akad. Nauk SSSR Geophiz. Inst.*, **24**, 163-187.

Monteith, J.L. (1965) Evaporation and environment. In Symposia of the Society for Experimental Biology.

NGWA (2009) The groundwater supply and its use. In http://wellowner2.org/2009/index.php?option=com_content&view=category&id=48&layout=blog&Itemid=46.

Parmesan, C. & Yohe, G. (2003) A globally coherent fingerprint of climate change impacts across natural systems. **421**, 37-42.

Penman, H.L. (1948) Natural evaporation from open water, bare soil and grass. In Proceedings of the Royal Society of London.

Pinol, J., Terradas, J., & Lloret, F. (1998) Climate Warming, Wildfire Hazard, and Wildfire Occurrence in Coastal Eastern Spain. *Climatic Change*, **38**, 345-357.

Raz Yaseef, N. (2008) Partitioning the evapotranspiration flux of the Yatir semi-arid forest. Ph.D., Weizmann Institute of Science, Rehovot.

Rees, W.G. (2001) *Physical principles of remote sensing*, second edn. Cambridge University Press, Cambridege, UK.

Sellers, P.J., Hall, F.G., Asrar, G., Strebel, D.E., & Murphy, R.E. (1992) An Overview of the First International Satellite Land Surface Climatology Project (ISLSCP) Field Experiment (FIFE). *J. Geophys. Res.*, **97**.

Sellers, P.J., Mintz, Y., Sud, Y.C., & Dalcher, A. (1986) A Simple Biosphere model (SiB) for use within general circulation models. *Journal of the Atmospheric Sciences*, **43**, 505-531.

Sellers, P.J., Randall, D.A., Collatz, G.J., Berry, J.A., Field, C.B., Dazlich, D.A., Zhang, C., Collelo, G.D., & Bounoua, L. (1996) A Revised Land Surface Parameterization (SiB2) for Atmospheric GCMs. Part I: Model Formulation. *Journal of Climate*, **9**, 676-705.

Shaw, R.H. & Pereira, A.R. (1982) Aerodynamic roughness of a plant canopy: A numerical experiment. *Agricultural Meteorology*, **26**, 51-65.

Snyder, W.C., Wan, Z., Zhang, Y., & Feng, Y.-Z. (1998) Classification-based emissivity for land surface temperature measurement from space. *International Journal of Remote Sensing*, **19**, 2753 - 2774.

Thom, A.S. (1972) Momentum, mass and heat exchange of vegetation. *Quarterly journal of the Royal Meteorological Society*, **98**, 124-134.

Thom, A.S. (1975). Momentum, mass and heat exchange of plant communities. In *Vegetation and the atmosphere, vol. I, Principles.* (ed J.L. Monteith). Academic Press, London.

Tiktak, A. & van Grinsven, H.J.M. (1995) Review of sixteen forest-soil-atmosphere models. *Ecological Modelling*, **83**, 35-53.

Verhoef, A. & Allen, S.J. (1998) The relative importance of surface and aerodynamic resistances in a multi-source energy-CO2 model. *Physics and Chemistry of The Earth*, **23**, 459-463.

WRI (2002) World Resource Institute. Drylands, people, and ecosystem goods and services: A web-based geospatial analysis. In http://www.wri.org/publication/content/8236.